

Self-interstitial atom defects in bcc transition metals: Group-specific trends

D. Nguyen-Manh,¹ A. P. Horsfield,² and S. L. Dudarev¹

¹EURATOM/UKAEA Fusion Association, Culham Science Centre, Oxfordshire OX14 3DB, United Kingdom

²Department of Physics and Astronomy, University College London, London WC1E 6BT, United Kingdom

(Received 24 October 2005; published 3 January 2006)

We present an investigation of systematic trends for the self-interstitial atom (SIA) defect behavior in body-centered cubic (bcc) transition metals using density-functional calculations. In all the nonmagnetic bcc metals the most stable SIA defect configuration has the $\langle 111 \rangle$ symmetry. Metals in group 5B of the periodic table (V, Nb, Ta) have significantly different energies of formation of the $\langle 111 \rangle$ and $\langle 110 \rangle$ SIA configurations, while for the group 6B metals (Cr, Mo, W) the two configurations are linked by a soft bending mode. The relative energies of SIA defects in the nonmagnetic bcc metals are fundamentally different from those in ferromagnetic bcc α -Fe. The systematic trend exhibited by the SIA defect structures in groups 5B and 6B transition metals correlates with the observed thermally activated mobility of SIA defects.

DOI: [10.1103/PhysRevB.73.020101](https://doi.org/10.1103/PhysRevB.73.020101)

PACS number(s): 61.80.Az, 66.30.Lw, 67.80.Mg, 71.15.Mb

Just as viruses at the time of their discovery more than a century ago¹ could not be visualized using the available optical instruments, so are individual point defects produced by irradiation in metals still inaccessible to direct imaging by modern electron microscopes.² Body-centered cubic (bcc) transition metals (TMs) and their alloys, including ferritic-martensitic steels, are prime candidate structural materials for fusion and advanced nuclear applications. Thus there is a well recognized need to have a quantitative understanding of the structure and formation energies of radiation defects in these materials³ to enable the development of predictive models of their microstructural evolution. A self-interstitial atom (SIA) defect is remarkably different from a vacancy because of the very large local strain field associated with the core of the defect. In the case of bcc TMs, the degree of linear compression in the core of a SIA defect approaches 20% (Ref. 4) and is well outside the range of approximations based on elasticity, thus other techniques are required to understand them.

The available experimental information on defects in bcc transition metals⁵ shows pronounced group-specific trends linked to the electron-to-atom ratio. In addition to the “anomalous self-diffusion” in the high-temperature bcc phases of group 4B (Ti, Zr, and Hf) metals,⁶ the mobility of vacancies in groups 5B and 6B elements,⁷ and of the $\langle 111 \rangle$ screw dislocations,⁸ is correlated with the elastic properties. While the formation and thermal migration energies of vacancies can be readily estimated from experiment, the large formation energies of SIA defects make them less accessible to a direct observation. The only systematic data on thermally activated migration of SIAs come from the analysis of resistivity recovery curves of materials irradiated by electrons. In the case of group 5B metals the resistivity recovery curves show that individual SIAs are already mobile at temperatures below 6 K for V, Nb, and Ta (Ref. 5). In other bcc TMs thermally activated migration of SIA defects starts at 40 K in Cr (Ref. 9), 35 K in Mo (Ref. 10), 27 K in W (Ref. 11), and 120 K in α -Fe (Ref. 12). So far it has proved difficult to formulate a consistent and systematic model explaining these trends.

Density-functional calculations (DFT) of vacancies in bcc transition metals have been reported.^{13,14} For interstitial con-

figurations it was initially assumed that empirical many-body interatomic potentials¹⁵ correctly predicted the $\langle 110 \rangle$ dumbbell as the most stable SIA configuration in all the bcc TMs except tungsten. This view is in agreement with the orthorhombic long-range distortions observed using x-ray Huang diffuse scattering in Mo and α -Fe at low temperatures.¹⁶ While recent DFT calculations^{17,18} and a tight-binding Stoner model¹⁹ confirmed the $\langle 110 \rangle$ dumbbell as the most stable SIA configuration in α -Fe, Han *et al.*²⁰ found that in V and Mo the $\langle 111 \rangle$ configuration had the lowest formation energy. Woo and Frank²¹ also emphasized the significance of the $\langle 111 \rangle$ configuration. This did not agree with the established views that “the $\langle 110 \rangle$ dumbbell has been widely accepted as the SIA configuration in Mo and other bcc metals.”¹⁰ Hence, despite a great body of existing work, there is still uncertainty in our understanding of the structure and basic properties of SIA defects in nonmagnetic bcc metals. In this paper we address the issue by means of a systematic *ab initio* investigation. By following the periodic table, we discover systematic trends in the *relative* energies of formation of various configurations of SIA defects. These trends help in identifying the origin of the different mechanisms of thermally activated migration of SIAs in metals of groups 5B and 6B.

Unless stated otherwise, all the calculations described in this Communication were carried out using the package of linear combination of atomic type orbitals (PLATO).²² Both volume and ionic relaxations were performed using a variable metric algorithm on $4 \times 4 \times 4$ cells containing $128(\pm 1)$ atoms. A $3 \times 3 \times 3$ Monkhorst-Pack k -point grid was found to be sufficient for obtaining accurate values of defect formation energies. The calculations were performed using relativistic semicore separable pseudopotentials²³ with the Perdew–Burke–Ernzerhof (PBE)²⁴ generalized gradient approximation (GGA) for the exchange and correlation functional. Valence and semicore electrons were described by a double numerical plus polarization (DNP) basis set that consists of 18 atomiclike functions per atom. For the nd ($n=3, 4, 5$) transition-metal series we keep the ns , np , nd , $(n+1)s$ orbitals for the neutral atom plus nd^* , $(n+1)s^*$, $(n+1)p^*$ orbitals for the ions of charge +2. The orbitals were cut off at a radius of 8.0 atomic units (a.u.), and their tails were

TABLE I. The first four rows are basic parameters of bcc transition metals evaluated using PLATO, with the experimental values taken from Refs. 26 and 5 in italics. The remaining rows are the formation energies (in eV) of SIA defects in groups 5B and 6B. The values given in italics are from Ref. 20 and those given in typescript font are from Ref. 15.

	V	Nb	Ta	Cr	Mo	W
a (Å)	3.04	3.32	3.31	2.85	3.17	3.18
	<i>3.03</i>	<i>3.30</i>	<i>3.30</i>	<i>2.88</i>	<i>3.15</i>	<i>3.16</i>
B (Mbar)	1.71	1.73	1.99	1.92	2.68	3.05
	<i>1.62</i>	<i>1.70</i>	<i>2.00</i>	<i>1.90</i>	<i>2.72</i>	<i>3.23</i>
H^v (eV)	2.51	2.99	3.14	2.64	2.96	3.56
	<i>2.1–2.2</i>	<i>2.6–3.1</i>	<i>2.8–3.1</i>	<i>2.0–2.4</i>	<i>2.6–3.2</i>	<i>3.5–4.1</i>
H_m^v (eV)	0.62	0.91	1.48	0.91	1.28	1.78
	<i>0.5–1.2</i>	<i>0.6–1.0</i>	<i>0.7–1.9</i>	<i>0.95</i>	<i>1.3–1.6</i>	<i>1.7–2.0</i>
$\langle 111 \rangle$	3.367	5.253	5.832	5.685	7.417	9.548
Dumbbell	<i>3.14</i>	4.795	7.157		<i>7.34</i>	8.919
$\langle 111 \rangle$	3.371	5.254	5.836	5.660	7.419	9.551
Crowdion	<i>3.15</i>	4.857	7.158		<i>7.34</i>	8.893
$\langle 110 \rangle$	3.652	5.597	6.382	5.674	7.581	9.844
	<i>3.48</i>	4.482	6.847		<i>7.51</i>	9.641
Tetrahedral	3.835	5.758	6.771	6.189	8.401	11.05
	<i>3.69</i>				<i>8.20</i>	
$\langle 100 \rangle$	3.918	5.949	7.003	6.643	9.004	11.49
	<i>3.57</i>	4.821	8.068		<i>8.77</i>	9.815
Octahedral	3.964	6.060	7.095	6.723	9.067	11.68
	<i>3.62</i>				<i>8.86</i>	

smoothed over a distance of about 1.5 a.u. The electron charge density was projected onto a uniform fast Fourier transform (FFT) mesh of spacing 0.2 a.u. The electrons were given an effective temperature of 0.2 eV. The forces and stress components in relaxed configurations were smaller than 0.025 eV/Å and 0.001 Mbars, respectively. To verify the accuracy of PLATO, we cross-checked the calculations with the Vienna *ab initio* simulation package (VASP) code,²⁵ where we used the projector augmented wave (PAW) approach with plane-wave cutoff energies in the range of 300–400 eV and the GGA-PBE exchange-correlation functional. There is always good agreement between PLATO and VASP data on defect formation energies and trends of the different SIA configurations. Results of benchmarking calculations for bulk properties of bcc TMs of groups 5B and 6B are summarized in Table I and compared with experimental data. In the case of Cr we assumed the nonmagnetic state the energy of which was very close to the energy of the antiferromagnetic (AFM) state.²⁷ The vacancy migration energies were found using the nudged elastic band method.²⁸ The values predicted by the PLATO code agree well with experimental data not only for the lattice constants and bulk moduli, but also for the monovacancy formation and migration energies.⁵ Table I provides a systematic set of calculated values of vacancy migration energies. Comparing these data with earlier DFT calculations,^{13,14} we find that our calculations show better overall agreement with the experiment.

Figure 1 shows the atomic structure and charge-density deformation maps for two relaxed SIA configurations: $\langle 111 \rangle$ dumbbell and $\langle 110 \rangle$ dumbbell. The darker color highlights atoms situated in the highly deformed core regions of the defect. The energy of the relaxed $\langle 111 \rangle$ dumbbell configuration, where two atoms share a lattice site, is very similar to those of the crowdion configuration, where four atoms share three lattice sites. In both configurations the deformation is largely confined to a single string of atoms running in the $[111]$ direction. The $\langle 110 \rangle$ dumbbell configuration is closely related to the $\langle 111 \rangle$ configuration since the pattern of deformation associated with the $\langle 110 \rangle$ dumbbell is effectively formed by two superimposed $\langle 111 \rangle$ -type SIA configurations. For each configuration we show the charge-density deformation maps that illustrate the link between the atomistic and electronic structure of a defect, and highlight the significance of directional bonding between atoms in the core of the defect.

Table I includes the calculated formation energies of SIA defects in all the TMs of groups 5B and 6B. The total systematic error in the calculations is of the order of 0.015 eV. We find that the $\langle 111 \rangle$ -type configurations have the lowest formation energies in all the nonmagnetic bcc metals with the $\langle 110 \rangle$ configuration being separated by an energy gap that is smaller in group 6B than in group 5B. The pattern of ordering of SIA configurations is fundamentally different from that of ferromagnetic bcc Fe, where the $\langle 110 \rangle$ configuration has the lowest formation energy.¹⁸ Our findings are at variance with defect formation energies predicted using the empirical many-body interatomic potentials¹⁵ for which the $\langle 110 \rangle$ dumbbell is the lowest energy SIA configuration. A notable exception to the rule is the Ackland and Thetford¹⁵ prediction of the stable $\langle 111 \rangle$ SIA configuration in W. However, the predicted $\langle 111 \rangle$ - $\langle 110 \rangle$ energy gap of 0.75 eV (Ref. 15) is three times that found in DFT calculations. For nonmagnetic Cr the difference between the crowdion and $\langle 110 \rangle$ configurations is exceedingly small. We find that the relative energies of SIA configurations follow the same pattern in all nonmagnetic bcc metals, namely that the $\langle 111 \rangle$ dumbbell or crowdion configuration is followed by the $\langle 110 \rangle$ dumbbell, and then by the tetrahedral, the $\langle 100 \rangle$, and the octahedral configurations. Table I provides, therefore, a complete and self-consistent DFT database of defect energies required for constructing more accurate interatomic potentials for modeling defects and dislocations in bcc TMs.

The group-specific trends in the SIA formation energies found in the present calculations are illustrated in Fig. 2 separately for metals of groups 5B and 6B and compared to those of ferromagnetic bcc Fe (Ref. 18). Figure 2 shows a striking dissimilarity in the pattern of ordering of energies of SIA defect configurations between the nonmagnetic bcc TMs and bcc Fe. The significance of the magnetic contribution to the energy of formation of SIA defects in ferromagnetic bcc Fe is also evident from recent DFT studies,^{17,18} where the most stable and relatively immobile $\langle 110 \rangle$ dumbbell owes its stability to magnetism lowering its energy by ~ 0.7 eV in comparison with the $\langle 111 \rangle$ configuration. The most notable trend is exhibited by the calculated formation energy differ-

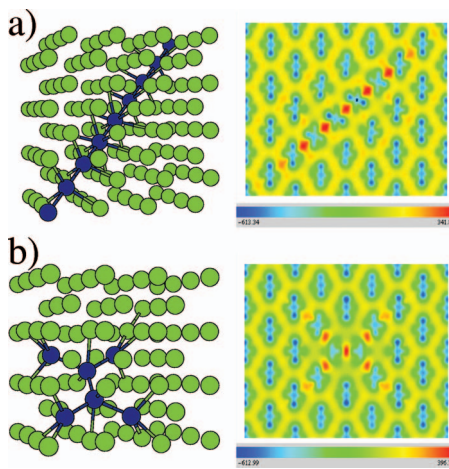


FIG. 1. (Color) Relaxed SIA configurations and the corresponding electronic charge-density (multiplied by cell volume) deformation maps on the $\langle 110 \rangle$ plane calculated (using VASP) by subtracting the final charge distributions from atomic charge densities for two SIA configurations: (a) $\langle 111 \rangle$ dumbbell and (b) $\langle 110 \rangle$ dumbbell, in a representative case of bcc Mo.

ence between the $\langle 110 \rangle$ and the $\langle 111 \rangle$ configurations of metals in group 5B that is consistently larger than those of corresponding elements in group 6B (0.29 eV for V in comparison with 0.01 eV for Cr, 0.34 eV for Nb with 0.16 eV for Mo, and 0.55 eV for Ta with 0.29 eV for W). Apart from the apparent differences between energies of the $\langle 110 \rangle$ and $\langle 111 \rangle$ configurations, all other SIA configurations in Fe follow the same *relative* pattern as SIA configurations in groups 5B and 6B.

The large energy differences between the $\langle 110 \rangle$ and $\langle 111 \rangle$ dumbbells make Ta and W good representative cases of groups 5B and 6B metals for investigating the migration pathways linking the $\langle 111 \rangle$, $\langle 110 \rangle$, and $\langle 100 \rangle$ defect configurations. The results obtained using the nudged elastic band method are shown in Fig. 3. While the transformation pathways linking the $\langle 111 \rangle$ and the $\langle 100 \rangle$ configurations (left panel) in the two metals exhibit a similar behavior, it is striking to see a qualitative difference between Ta and W in the

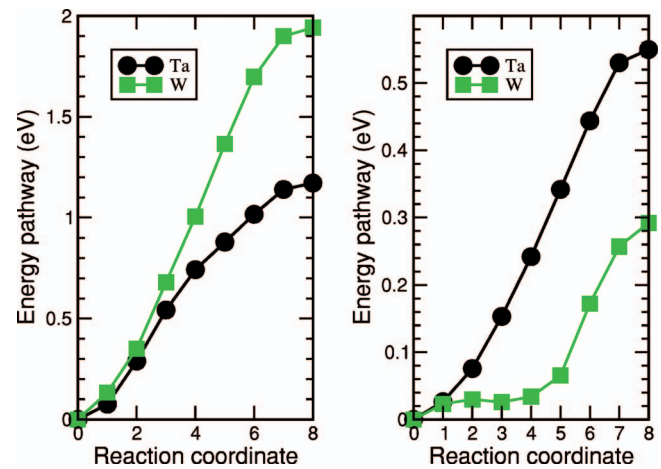


FIG. 3. (Color) Energy pathways between the $\langle 111 \rangle$ and $\langle 100 \rangle$ dumbbells (left) and between the $\langle 111 \rangle$ and $\langle 110 \rangle$ dumbbells (right) for bcc Ta and bcc W.

shape describing the $\langle 111 \rangle$ to $\langle 110 \rangle$ transition (right panel). While in W the $\langle 111 \rangle$ defect is characterized by the presence of a fairly soft deformation mode transforming it into a $\langle 110 \rangle$ dumbbell, in Ta the $\langle 111 \rangle$ defect is rigid and stable with respect to the $\langle 111 \rangle$ to $\langle 110 \rangle$ transition. We note that “bent” SIA configurations were investigated by Han *et al.*²⁰ and, earlier, by Ackland and Thetford¹⁵ in the case of bcc Mo. The important difference between a bent configuration found using the empirical many-body potentials¹⁵ and the soft bending mode found in DFT calculations is that the $\langle 111 \rangle$ configuration still has the lowest formation energy. Since the three bending modes (corresponding to each of the three 110 planes intersecting along the diagonal of bcc lattice) are easily excited even at low temperatures, they give rise to the high relative statistical weight of planar $\langle 110 \rangle$ -like configurations observed in x-ray diffuse scattering experiments.¹⁶ The presence of soft bending modes should be expected to have a significant effect on the mobility of defects. Due to the smaller difference between the energies of the $\langle 111 \rangle$ and $\langle 110 \rangle$ configurations the existence of these modes should have a more pronounced effect on the mobility of defects in

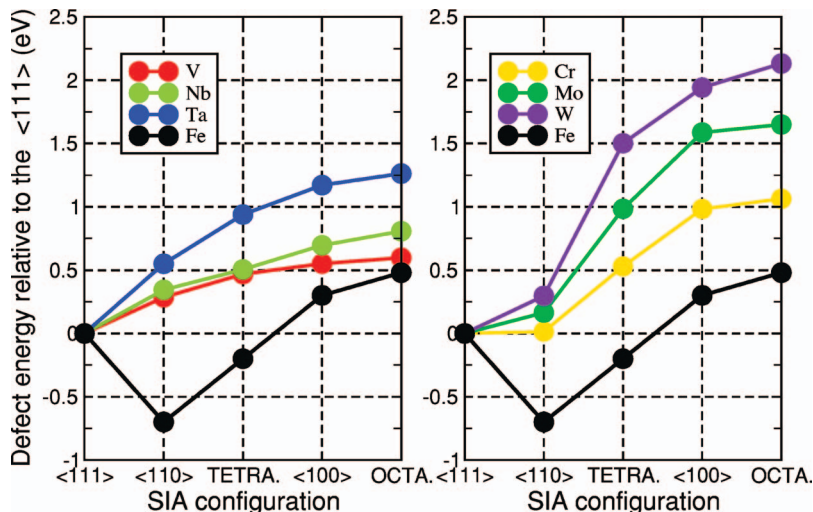


FIG. 2. (Color) Formation energies of several basic SIA configurations calculated for bcc TMs of group 5B (left) and group 6B (right). Data for bcc Fe is taken from Ref. 18.

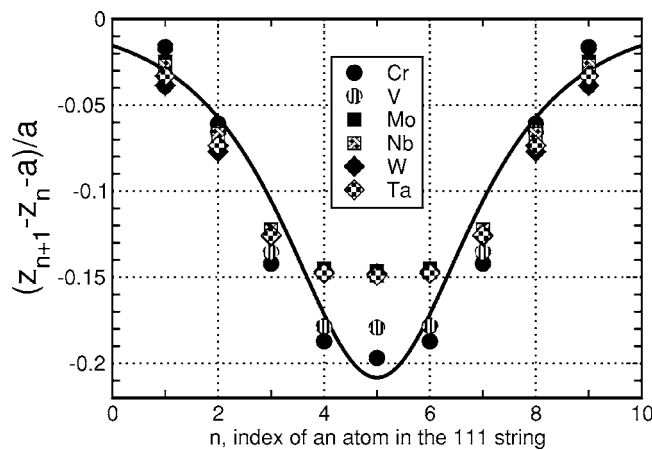


FIG. 4. Fields of atomic displacements in the central string of the crowdion configuration evaluated for bcc metals. The solid line shows the soliton solution of the sine-Gordon equation (Ref. 4) $z_n = (2a/\pi)\arctan\{\exp[-(n-n_0)/N]\}$ plotted for the effective dimensionless width $N=1.5$ and the position of the center of the crowdion $n_0=5.5$; $a=(\sqrt{3}/2)a_0$, where a_0 is lattice constant.

Cr than in W. This observation agrees with the trend exhibited by the stage 1 temperatures in group 6B metals that increase from 27 K in W to 40 K in Cr (Ref. 7). Hence we should expect that while in group 5B metals the $\langle 111 \rangle$ SIA configurations perform one-dimensional (1D) Brownian motion in the direction of their axis, the mobility of defects in

group 6B metals is affected by the soft bending modes impeding thermally activated 1D migration.

Our study shows that the $\langle 111 \rangle$ configuration represents the most stable SIA defect in all the nonmagnetic bcc metals. This configuration is approximately described by the exactly solvable sine-Gordon model⁴ in which the field of atomic displacements in the core of the defect is given by a universal function of atomic coordinates. Figure 4 shows atomic displacements calculated for the $\langle 111 \rangle$ strings of atoms using the crowdion configurations found in all the six metals of groups 5B and 6B. We find the strongest deformation occurring in the core of SIA defects in $3d$ TMs (V and Cr), while in the case of $4d$ and $5d$ TMs the defects have more extended cores. This observation suggests that core electrons play a more significant part in determining the structure and the energies of formation of SIA defects in $4d$ and $5d$ TMs. Figure 4 also shows that the field of atomic displacement does have a universal structure, which away from the central core region agrees with the solution of the sine-Gordon model. Interestingly, the calculated values of migration energy for a nearest-neighbor translation of the defect in the $\langle 111 \rangle$ direction are 0.03 and 0.05 eV for Ta and W that are in good agreement with the experimental values of 0.033 (Ref. 29) and 0.054 eV (Ref. 11), respectively.

We acknowledge stimulating discussions with I. Cook, J. Evans, S. Kenny, S. Han, Y. Osetsky, M. Victoria, and C. H. Woo. This work was funded by the EXTREMAT Project, by EURATOM, and by the UK-EPSRC.

- ¹D. Ivanovsky, *Bull. Acad. Imp. Sci. St. Pétersbourg* **35**, 67 (1892); M. W. Beijerinck, *Verh.-K. Ned. Akad. Wet., Afd. Natuurkd., Eerste Reeks* **65**, Sect. 2, Deel 6, 3 (1898).
- ²M. L. Jenkins and M. A. Kirk, *Characterisation of Radiation Damage by Transmission Electron Microscopy* (Institute of Physics, Bristol, 2001).
- ³S. J. Zinkle, *Phys. Plasmas* **12**, 058101 (2005).
- ⁴S. L. Dudarev, *Philos. Mag.* **83**, 3577 (2003).
- ⁵P. Ehrhart, P. Jung, H. Schultz, and H. Ullmaier, in *Atomic Defects in Metals*, edited by H. Ullmaier, Landolt-Börnstein, New Series, Group III, Vol. 25 (Springer-Verlag, Berlin, 1991).
- ⁶J. N. Mundy, *Defect Diffus. Forum* **83**, 1 (1992).
- ⁷H. Shultz, *Mater. Sci. Eng., A* **141**, 149 (1991).
- ⁸M. S. Duesbury and V. Vitek, *Acta Mater.* **46**, 1481 (1998).
- ⁹M. Weller and P. Moser, *J. Phys. (Paris), Colloq.* **42**, C5-741 (1981).
- ¹⁰J. H. Evans, EURATOM/UKAEA Fusion Report No. 499 (2003) (unpublished).
- ¹¹F. Dausinger and H. Schultz, *Phys. Rev. Lett.* **35**, 1773 (1975).
- ¹²S. Tanaka, J. Fuss, H. Kugler, U. Dedek, and H. Schultz, *Radiat. Eff.* **79**, 87 (1983).
- ¹³P. Söderlind, L. H. Yang, J. A. Moriarty, and J. M. Wills, *Phys. Rev. B* **61**, 2579 (2000).
- ¹⁴F. Willaime, A. Satta, M. Nastar, and O. Le Bacq, *Int. J. Quantum Chem.* **77**, 927 (2000).
- ¹⁵G. J. Ackland and R. Thetford, *Philos. Mag. A* **56**, 15 (1987).
- ¹⁶P. Ehrhart, K. H. Robrock, and H. R. Schober, in *Physics of*

Radiation Effects in Crystals, edited by R. A. Johnson and A. N. Orlov (Elsevier, Amsterdam, 1986).

- ¹⁷C. Domain and C. S. Becquart, *Phys. Rev. B* **65**, 024103 (2002).
- ¹⁸C. C. Fu, F. Willaime, and P. Ordejon, *Phys. Rev. Lett.* **92**, 175503 (2004).
- ¹⁹G. Liu, D. Nguyen-Manh, B.-G. Liu, and D. G. Pettifor, *Phys. Rev. B* **71**, 174115 (2005).
- ²⁰S. Han, L. A. Zepeda-Ruiz, G. J. Ackland, R. Car, and D. J. Srolovitz, *Phys. Rev. B* **66**, 220101(R) (2002).
- ²¹C. H. Woo and W. Frank, *J. Nucl. Mater.* **137**, 7 (1985).
- ²²S. D. Kenny, A. P. Horsfield, and H. Fujitani, *Phys. Rev. B* **62**, 4899 (2000); K. Kohary, V. M. Burlakov, D. G. Pettifor, and D. Nguyen-Manh, *ibid.* **71**, 184203 (2005).
- ²³C. Hartwigsen, S. Goedecker, and J. Hutter, *Phys. Rev. B* **58**, 3641 (1998).
- ²⁴J. P. Perdew, K. Burke, and M. Ernzerhof, *Phys. Rev. Lett.* **77**, 3865 (1996).
- ²⁵G. Kresse and J. Hafner, *Phys. Rev. B* **47**, R558 (1993); G. Kresse and J. Furthmüller, *ibid.* **54**, 11169 (1996).
- ²⁶C. Kittel, *Introduction to Solid State Physics*, 5th ed. (Wiley, New York, 1976).
- ²⁷D. A. Pankhurst, D. Nguyen-Manh, and D. G. Pettifor, *Phys. Rev. B* **69**, 075113 (2004).
- ²⁸H. Johnson, G. Mills, and K. W. Jacobsen, in *Classical and Quantum Dynamics in Condensed Phase Simulations*, edited by B. J. Berne, G. Ciccootti, and D. F. Coker (World Scientific, Singapore, 1998), p. 385.
- ²⁹F. W. Young, *J. Nucl. Mater.* **69/70**, 310 (1978).